Scripta Materialia 211 (2022) 114484

Contents lists available at ScienceDirect

Scripta Materialia

journal homepage: www.elsevier.com/locate/scriptamat

Viewpoint set

3D local atomic structure evolution in a solidifying Al-0.4Sc dilute alloy melt revealed in operando by synchrotron X-ray total scattering and modelling

Shi Huang[a], Shifeng Luo[a,b], Ling Qin[a], Da Shu[c], Baode Sun[c], Alexander J G Lunt[d], Alexander M Korsunsky[e], Jiawei Mi[a,c,*]

[a] Department of Engineering, University of Hull, Cottingham Road, Hull HU6 7RX, United Kingdom
[b] School of Materials Science and Engineering, Hefei University of Technology, 193 Tunxi Road, Hefei 230009, China
[c] Shanghai Key Lab of Advanced High-temperature Materials and Precision Forming, School of Materials Science and Engineering, Shanghai Jiao Tong University, 800 Dongchuan Road, Shanghai 200240, China
[d] Department of Mechanical Engineering, University of Bath, Claverton Down, Bath, Somerset BA2 7AY, United Kingdom
[e] Department of Engineering Science, University of Oxford, Parks Rd, Oxford OX1 3PJ, United Kingdom

ARTICLE INFO

Article history:
Received 25 August 2021
Revised 17 December 2021
Accepted 21 December 2021
Available online 9 January 2022

Keywords:
Aluminium-Scandium alloy, Synchrotron X-ray total scattering
Empirical Potential Structure Refinement
Liquid Atomic Structure
In Operando Study of Solidification

ABSTRACT

Using synchrotron X-ray total scattering and empirical potential structure refinement modelling, we studied systematically in operando condition the disorder-to-order local atomic structure transition in a pure Al and a dilute Al-0.4Sc alloy melt in the temperature range from 690 °C to 657 °C. In the liquid state, icosahedral short-range ordered *Sc*-centred Al polyhedrons form and most of them with Al coordination number of 10–12. As the melt is cooled to the semisolid state, the most *Sc*-centred polyhedrons become more connected atom clusters via vertex, edge and face-sharing. These polyhedrons exhibit partially icosahedral and partially face-centred-cubic symmetry. The medium-range ordered *Sc*-centred clusters with face-sharing are proved to be the "precursors" of the $L1_2$ Al_3Sc primary phases in the liquid-solid coexisting state.

In a material system, the dynamic transition of atomic structure from a disordered state to an ordered state is a fundamental issue central to physics, chemistry and materials science. A quantitative and precise description of atom arrangement in 3D space, and how atoms move or rearrange themselves under a thermodynamic driving force (temperature, force, stress, etc.) is the basis for understanding phase change and the physical, chemical and mechanical property of a material. The liquid-to-solid phase transition is the most common structure transformation occurring in natural and man-made materials driven by the change of temperature [1–4]. Quantitative understanding of the temperature-driven atomic structure evolution is scientifically [5] and technologically [6] important for alloy design, development and optimization. For disordered-to-ordered atomic structure transition in liquid Al based metal alloys, the icosahedral short-range ordered (ISRO) structure has been widely considered as one of the intermediate geometry configuration between the disordered and ordered states. For example, in Al alloys added with transitional metal elements, Simonet and Holland-Moritz found the ISRO structures in the melts of Al-Pb-Mn [7], Al-Mn-Cr [8] and Al-Cu-Co [9] using neutron scattering and simulation. Molecular dynamics simulations also showed the existence of icosahedra in an Al-Sm [10,11] and an Al-Cu [12] alloy. Their phase fraction decreased as the crystalline FCC clusters increased during the subsequent crystallization process. Unfortunately, most simulation work lacks direct experimental evidence and validation. Robust real-time experiments plus experimentally validated 3D atomic structure simulation are essential for revealing and elucidating the evolution of atomic structure in transition from the liquid to solid state, and how new phases are nucleated in the undercooled liquid or liquid-solid coexisting state that is meaningful to industry practice.

In addition, until now, almost all previous experimental studies on Al-based alloys used relatively high percentage (in excess of 10%) of solute elements, for example, $Al_{87.5}Fe_{12.5}$ [13], $Al_{80}Ni_{20}$ [14] and $Al_{86}Cu_{14}$ [15]. Such a high level of solute elements would result in the formation of detrimental or undesired intermetallic phases in most commercial alloy systems, except in some cases of specially designed high/medium entropy alloys [16] . For those elements added as grain refiners to Al alloys, e.g. Ti, Zr, *Sc*, the con-

* Corresponding author.
E-mail address: j.mi@hull.ac.uk (J. Mi).

https://doi.org/10.1016/j.scriptamat.2021.114484

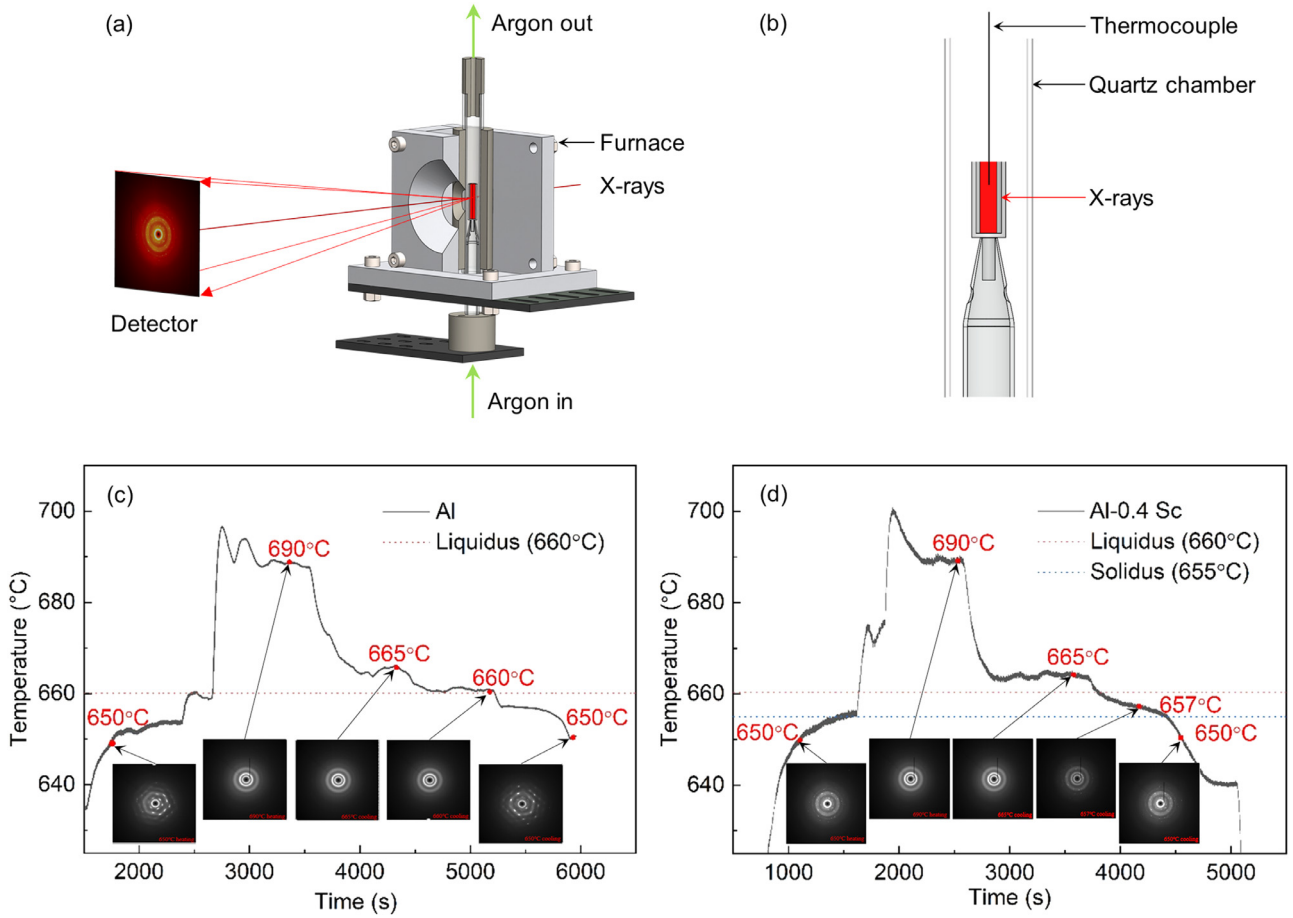

Fig. 1. (a) The specially designed apparatus used for the synchrotron X-ray total scattering in operando experiments. A half of the front part is opened up to illustrate more clearly the furnace, arrangement of the metal sample and quartz tube sample holder. (b) The location where the K-type thermocouple tip was inserted inside the melt, and the point where scattering patterns were taken. (c) and (d) show the measured temperature profiles and the 2D scattering patterns acquired at the target temperatures during heating and cooling for a pure Al sample, and (d) an Al-0.4Sc sample respectively.

tent is normally < 0.5wt% [5]. Therefore, an in-depth study and understanding of the dynamic interaction between Al atoms and the dilute alloy elements in the liquid and liquid-solid coexisting state are scientifically important. In this aspect, *Sc* and the primary Al_3Sc phases formed in the Al melt [17,18] are also technologically important, because *Sc* has been known as the best heterogenous grain refiner, the most potent suppressor for recrystallization and the strongest hardener for aluminium alloys [19,20]. Although some studies [21] on characterizing the 2D and 3D structure of Al_3Sc phases have been made, a precise understanding of how the primary Al_3Sc phase forms from a disordered liquid structure to its crystalline structure has not been seen reported.

In this letter, the disordered-to-ordered atomic structure transition in a dilute Al-0.4wt% *Sc* alloy melt at different temperatures was studied. Synchrotron X-ray total scattering (SXTS) and empirical potential structure refinement (EPSR) method were used to study the atomic structure of the liquid Al and Al-0.4 wt% *Sc* alloys in the temperature range from 690 °C down to 657 °C. The objective was to elucidate precisely the temperature-dependant atomic structure evolution in the temperature region where undercooled liquid and solid co-exist, a condition where active alloy structure control measure and processing techniques can be applied for optimising alloy design, structure and manufacturing.

The SXTS experiments were carried out at the beamline I15 of Diamond Light Source (DLS), UK. A monochromatic X-ray of 50.239 KeV and a 2D flat-panel Si detector (Perkin-Elmer 1621) were used to acquire the scattering patterns. The experimental apparatus (furnace), sample arrangement and temperature measurement are shown in Fig. 1a and Fig. 1b. The measured temperature profiles and diffraction (scatterring) patterns are indicated in Fig. 1c and Fig. 1d. More detailed information about the furnace design and experimental parameters are described in the S1 section of supplementary materials. At each target temperature, the melt was held there for sufficient time to homogenize the temperature before taking scattering pattern. 240 s exposure time was used for each pattern. After the pattern was taken, the temperature change was within ±1 °C of the target temperature. Bragg spots due to the formation of crystalline phases appeared in the scattering patterns for samples cooled below the liquidus. To extract the scattering information from the remaining liquid melt only, an adaptive method was used to remove the Brag spots from the patterns, similar to that used in [22]. Calibration and conversion of the 2D patterns into 1-D intensity profile were carried out using Fit2D [23] after background subtraction and data correction by using GudrunX [24]. The detailed procedures are described in the S2 section of supplementary materials (Fig. S2 and Table S1).

The EPSR package version 25 was used to reconstruct the 3D atomic structures according to the SXTS data and then extract the partial pair distribution functions (PDFs) from the total PDFs at each temperature. The EPSR started with refining a starting interatomic potential and then moving the positions of the atoms to produce the best possible agreement between the simulated and the measured structure factors [25]. The reference potential between an arbitrary atom pair (atom α and β) is a combination of

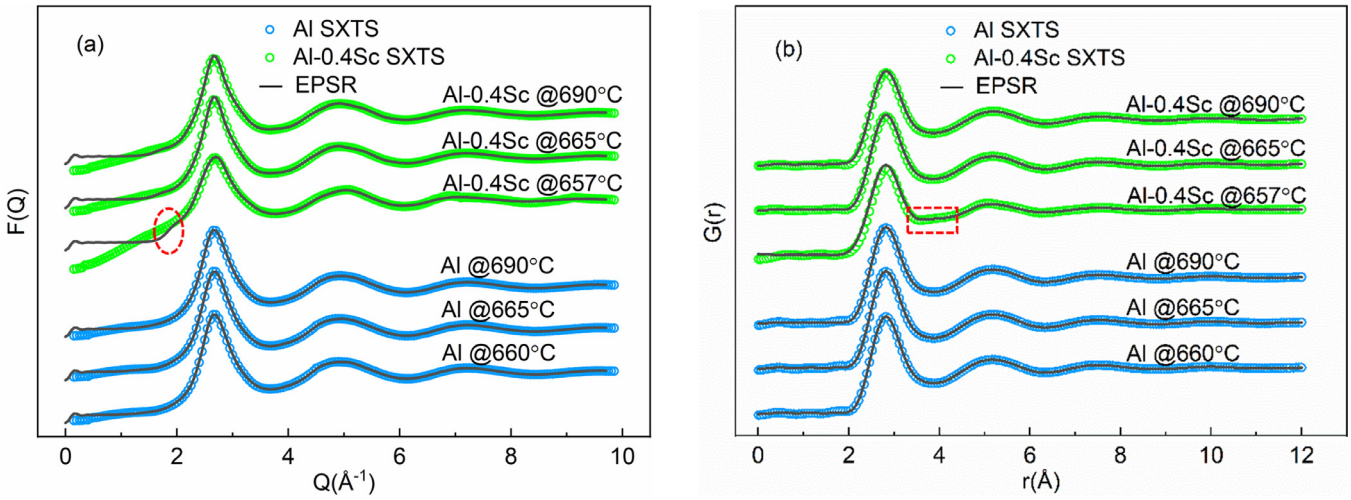

Fig. 2. The experimental and EPSR simulated (a) structure factors, F(Q); and (b) total PDFs, G(r) for the liquid Al and Al-0.4Sc melt at different temperatures.

Lennard-Jones and Coulomb potentials as below:

$$U_{\alpha\beta} = 4\varepsilon_{\alpha\beta}\left[\left(\frac{\sigma_{\alpha\beta}}{r}\right)^{12} - \left(\frac{\sigma_{\alpha\beta}}{r}\right)^{6}\right] + \frac{1}{4\pi\varepsilon_0}\frac{q_\alpha q_\beta}{r},$$

Where $\varepsilon_{\alpha\beta} = \sqrt{\varepsilon_\alpha \varepsilon_\beta}$ $\sigma_{\alpha\beta} = 0.5(\sigma_\alpha + \sigma_\beta)$, and ε_0 is the permittivity of free space. $\varepsilon_{\alpha\beta}$ is the well depth parameter, $\sigma_{\alpha\beta}$ is the range parameter, q_α and q_β are Coulomb charges of atom α and β.

The Lennard-Jones parameters used for the Al and *Sc* atoms are listed in Table S2 in supplementary materials. In this work, a cubic simulation domain with side length of 68.1 Å was used for the EPSR modelling. The atomic density and atom number information is listed in Table S3. The partition of *Sc* in the Al-0.4Sc melt at different temperatures was calculated according to the lever rule [26,27] in equilibrium condition. The detailed running steps of EPSR were described in [28]. The simulation was performed using one of the dedicated computing nodes (2 × 14-core Broadwell E5–2680v4 processors (2.4–3.3 GHz), 128 GB DDR4 RAM) of Hull University supercomputing cluster, Viper. It takes approximately 5 h of computing time (~5000 iterations) to complete a typical simulation with a satisfactory R-factor of $<10^{-3}$.

Fig. 2. shows the structure factor [F(Q)], and PDF [G(r)] obtained from the SXTS experiments and the corresponding EPSR modelling at different temperatures for both alloys. The simulated results matched the experimental data very well. A pre-peak appeared at ~1.8 $Å^{-1}$ in the F(Q) of the Al-0.4Sc alloy at 657 °C (red dashed circle in Fig. 2a). Correspondingly, there is minor shoulder appeared at ~4.0 Å of the G(r).

Fig. 3 shows the partial PDFs obtained from the EPSR modelling for both alloys at different temperatures. In the liquid Al melt, the first peak position of the $g(r)_{Al\text{-}Al}$ remained almost at the same r value while the peak height increased slightly as the temperature decreased (Fig. 3a), indicating that the melt structure gradually became more ordered as the melt was cooled. Fig. 3b and c show the partial PDFs of the Al-Al and Al-*Sc* pairs in the Al-0.4Sc melt, respectively. As the temperature decreased from 690 °C to 657 °C, the 1st peak position of $g(r)_{Al\text{-}Al}$ moved from ~2.79 Å to ~2.82 Å, while that of the $g(r)_{Al\text{-}Sc}$ moved from 2.61 Å to 2.58 Å (Fig. 3c). Simultaneously, a minor shoulder appeared at ~4.0 Å in the $g(r)_{Al\text{-}Al}$ at 657 °C (framed by a red dashed rectangle in Fig. 3b).

To study the Al atom configuration around an arbitrary reference *Sc* atom at different temperatures, the Al atoms in the first neighbouring shell were extracted from the EPSR models at the three different temperatures (see Figs. 4a, b, c and the accompanying video 1). In liquid state at 690 °C, the *Sc*-centred atom clus-

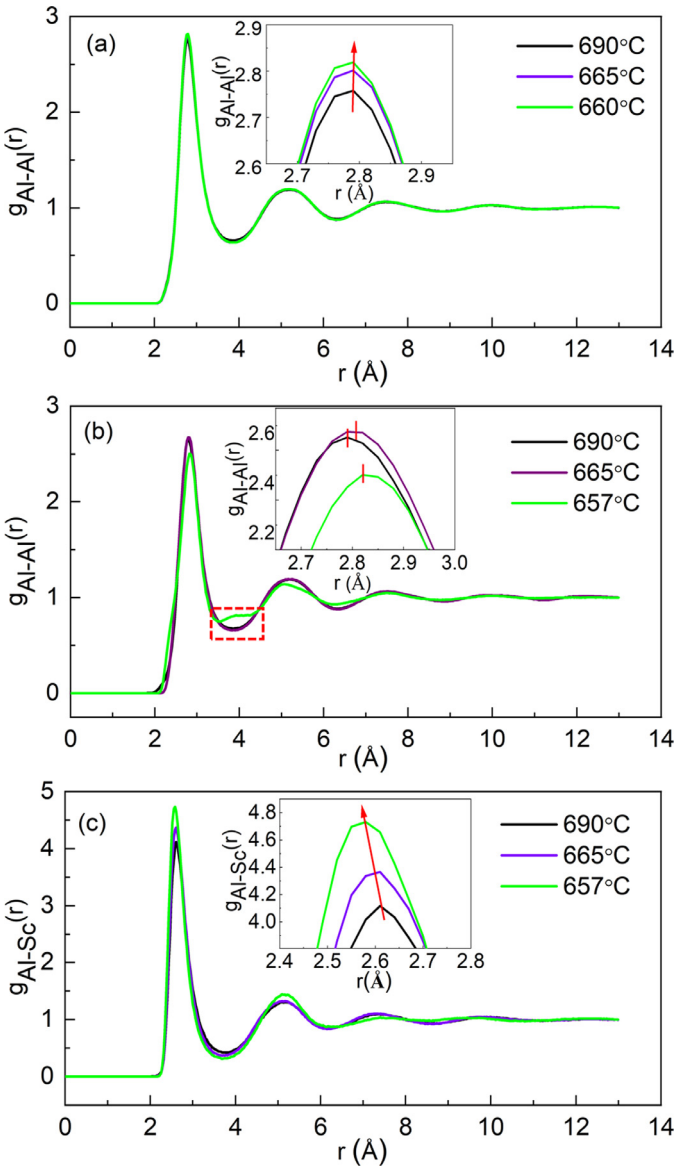

Fig. 3. (a) The PDFs of the Al-Al pair obtained from the EPSR modelling in pure liquid Al at different temperatures. (b) The partial PDFs of the Al-Al pair and (c) Al-*Sc* pair in the Al-0.4Sc melt at different temperatures.

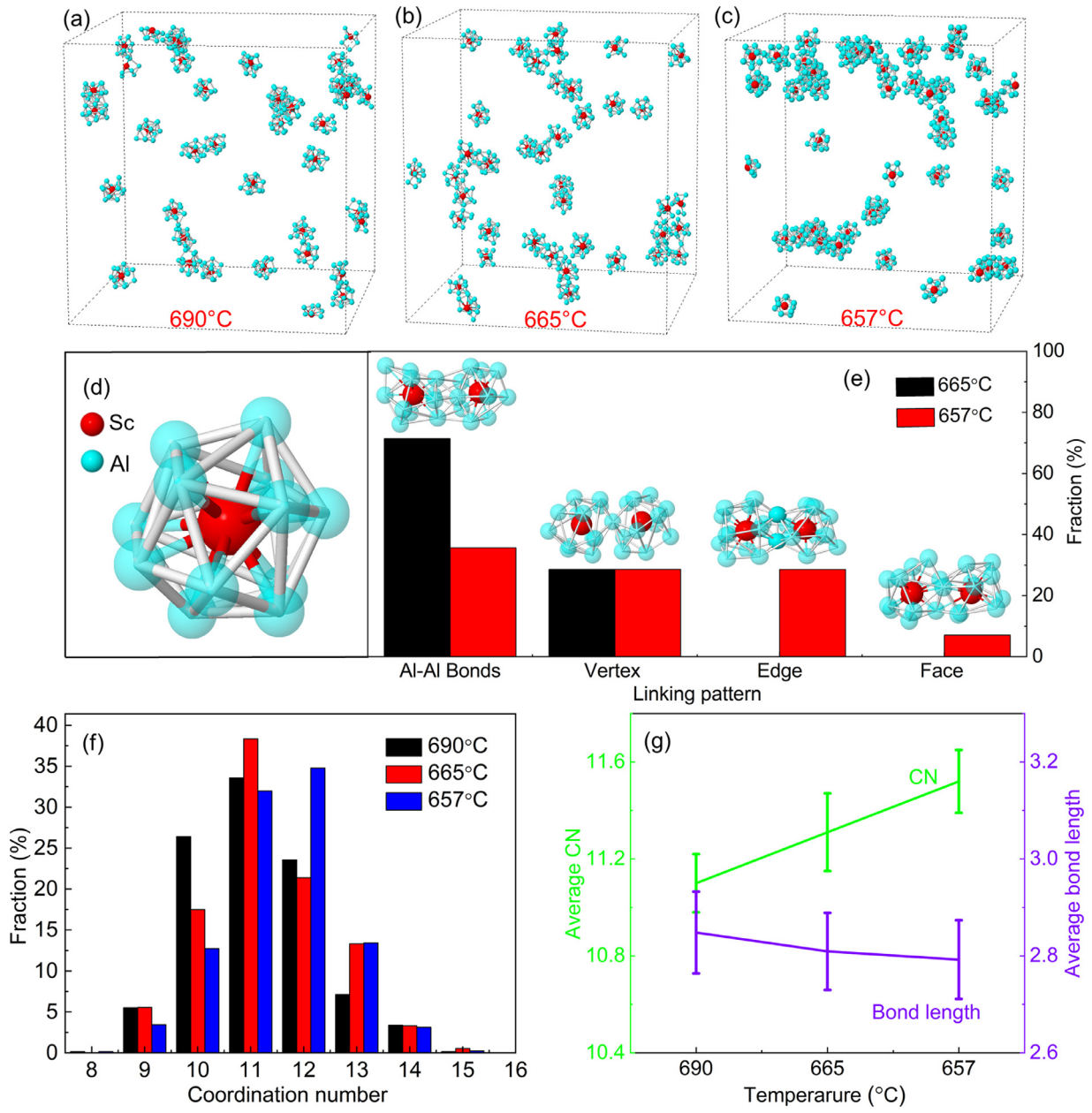

Fig. 4. The *Sc*-centred Al atom clusters in the Al-0.4Sc melt at (a) 690 °C, (b) 665 °C and (c) 657 °C respectively extracted from the EPSR models. (d) An enlarged view of a *Sc*-centred Frank-Kasper polyhedra with coordination number (CN) of 12 for the Al-0.4Sc melt at 690 °C. (e) Four different type medium-range ordered structures (MROs) formed by sharing the Al-Al bond, vertex, edge, and face between the neighbouring clusters. (f) The CN distribution of the *Sc* atoms in the Al-0.4Sc melt at 690 °C, 665 °C and 657 °C respectively. (g) the average CN and average bond length of the Al-*Sc* atom pair as a function of temperature.

ters (named as *Sc*-centred polyhedrons) were more sparsely distributed. A zoom-in view of an individual cluster (see Fig. 4d) indicated that it is a Frank-Kasper type polyhedral (full-icosahedra, <0, 0, 12, 0>). Some also exhibited the characteristics of fragmented icosahedra and icosahedra-like polyhedra with five-fold bonds. Hence, there are some ISRO in *Sc* coordination environment in liquid state [29]. After cooled from 665 °C to 657 °C, the *Sc*-centred polyhedrons moved closer to each other, starting to link together via the Al-Al bonds (without any sharing Al atom), vertex, edge and/or face sharing (without inter-penetration) [30], and forming four different configurations [31] as illustrated by the inserts in Fig. 4e. The Al-Al bonds connected configuration was dominant at 665 °C with 71.4%. It decreased to 35.7% at 657 °C. Edge-sharing and face-sharing connected configurations appeared at 657 °C, indicating more atoms were connected together as cooling proceeded. Fig. 4f shows the coordination number (CN) distribution of the *Sc*-centred polyhedrons at different temperatures. Clearly, at 690 °C and 665 °C, the peak value is at CN=11. While at 657 °C, the peak value is at CN=12. Fig. 4g also shows that, as the temperature decreased, the average CN increased from 11.1 to 11.52; while the mean bond length of the Al-*Sc* atom pairs decreased from 2.85 Å to 2.79 Å, indicating these *Sc*-centred polyhedrons become more compact.

A number of previous studies on the liquid melt structures of different Al-TM alloys [13–15] have found that the addition of 10∼20 wt% TM elements (for example, 12.5wt%Fe in [13], 20wt% Ni in [14] and 14wt%Cu in [15]) indeed changed the local atomic structures. In our research here, the addition of 0.4wt% *Sc* in Al

did not result in an obvious change in the F(Q) and G(r) profiles in the liquid state (690 °C) when compared to those of the pure liquid Al. However, in the semisolid range at 657 °C, a minor shoulder did appear at ~4 Å in the G(r) and $g(r)_{Al\text{-}Al}$ (corresponding to the pre-peak of F(Q) at ~1.8 $Å^{-1}$). Compared to the G(r) peak located at ~4.1 Å from the reference crystalline FCC phase reported in Fig. 4e of [11] and that of the pure Al at 900 K reported in Fig. 4a of [32], the minor shoulder indicated the formation of some medium-range FCC coordinated clusters in the semisolid melt. Such medium-range atom clusters have close geometry similarity to the equilibrium FCC crystal, and it can be called as medium-range crystalline order (MRCO) [33]. Fig. 4 illustrates that, as the temperature decreased, sparsely distributed *Sc*-centred polyhedrons became more connected with higher percentage of edge-sharing and face-sharing between the *Sc*-centred polyhedrons. Compared to the connection of icosahedra often reported in metallic glass systems [30], there was no volume-sharing connection between the *Sc*-centred polyhedrons. The bond orientational order parameter (see Fig. S3a) and Voronoi analysis (see Fig. S3b) results show that the *Sc*-centred polyhedrons exhibit partially icosahedral and partially FCC-like structure symmetry due to the geometric frustration which are the intermediate geometry configuration states (actually a distorted icosahedron configuration) between the two densely packed configurations, i.e. $L1_2$ crystalline order versus ISRO. This kind of geometry frustration was often attributed to the competition between two low-energy states ($L1_2$ and icosahedron) with dense atomic packing as widely reported in metallic glass, undercooled pure Al and Sm-doped liquid Al [10,11,34]. The formation of primary $L1_2$ ordered Al_3Sc phase indicates that $L1_2$ order wins over ISRO under the slow cooling condition. An ISRO compromise is generally required to minimize the total energy of 12 Al atoms surrounding a transition metal atom. While quantitative total energy calculation showed that ISRO compromise is not necessary for Al-*Sc* alloy. Substitutional FCC structure also satisfies the low total energy requirement [35], and the FCC symmetry is the energetically and geometrically favourable arrangement for the distorted parts of icosahedron [34]. Importantly, the local translational symmetry of the FCC configuration makes the distorted icosahedra easy to geometrically match with neighbouring clusters for long-range dense packing. In the liquid-solid coexisting region (657 °C), *Sc*-centred polyhedrons form medium-range order via face-sharing, the same type of connection exists in the FCC long-range packing Al_3Sc primary phase. Hence, the medium-range order *Sc*-centred clusters are the $L1_2$ precursors that form small ordered $L1_2$ clusters at the solid-liquid interface with low free-energy barrier for nucleation [36], and subsequently grow into Al_3Sc phases with a $L1_2$ structure.

The evolutions of 3D local atomic structures of an Al and an Al-0.4Sc alloy melt from liquid to liquid-solid coexisting state were studied in situ and in real time using synchrotron X-ray total scattering and EPSR modelling. In the liquid state, icosahedral short-range ordered *Sc*-centred Al polyhedrons form and most of them with Al coordination number of 10–12. As the melt is cooled to semisolid state, the polyhedrons become more connected atom clusters via vertex, edge and face-sharing. The medium-range ordered *Sc*-centred clusters with face-sharing are proved to be the "precursors" for the $L1_2$ Al_3Sc primary phase in the liquid-solid coexisting region.

Declaration of Competing Interest

The authors declare that they have no known competing financial interests or personal relationships that could have appeared to influence the work reported in this paper.

Acknowledgements

The authors would like to acknowledge the synchrotron X-ray beam time awarded by beamline I15 of Diamond Light Source (experimental No. EE20883-1); access to the University of Hull Supercomputer, Viper, and the technical support. Da Shu and Baode Sun also would like to acknowledge the financial support from the National Natural Science Foundation of China (Nos. U1832183 and 51821001). Shi Huang and Shifeng Luo also would like to acknowledge the financial support from the China Scholarship Council for their PhD study at University of Hull.

Supplementary materials

Supplementary material associated with this article can be found, in the online version, at doi:10.1016/j.scriptamat.2021.114484.

References

[1] H. Reichert, O. Klein, H. Dosch, M. Denk, V. Honkimäki, T. Lippmann, G. Reiter, Nature 408 (6814) (2000) 839–841.
[2] M. Guerdane, H. Teichler, B. Nestler, Phys. Rev. Lett. 110 (8) (2013) 086105.
[3] L. Xiong, X. Wang, Q. Yu, H. Zhang, F. Zhang, Y. Sun, Q. Cao, H. Xie, T. Xiao, D. Zhang, Acta Mater 128 (2017) 304–312.
[4] D.G. Eskin, J. Mi, Solidification processing of metallic alloys under external fields, Spinger Series in Materials Science 273, Springer Nature Switzerland AG, Cham Switzerland (2018) 1–320, doi:10.1007/978-3-319-94842-3.
[5] R.G. Guan, D. Tie, Acta Metall. Sin-Engl. 30 (5) (2017) 409–432.
[6] R. Zhang, S. Zhao, C. Ophus, Y. Deng, S.J. Vachhani, B. Ozdol, R. Traylor, K.C. Bustillo, J. Morris, D.C. Chrzan, Sci. Adv. 5 (12) (2019) eaax2799.
[7] V. Simonet, F. Hippert, H. Klein, M. Audier, R. Bellissent, H. Fischer, A.P. Murani, D. Boursier, Phys. Rev. B 58 (10) (1998) 6273.
[8] V. Simonet, F. Hippert, M. Audier, R. Bellissent, Phys. Rev. B 65 (2) (2001) 024203.
[9] D. Holland-Moritz, T. Schenk, V. Simonet, R. Bellissent, P. Convert, T. Hansen, D. Herlach, Mater. Sci. Eng. A 375 (2004) 98–103.
[10] X.W. Fang, C.Z. Wang, Y.X. Yao, Z.J. Ding, K.M. Ho, Phys. Rev. B 83 (22) (2011) 224203.
[11] D. Choudhuri, B.S. Majumdar, Materialia 12 (2020) 100816.
[12] Q. Zhang, J. Li, S. Tang, Z. Wang, J. Wang, J. Phys. Chem. C 125 (6) (2021) 3480–3494.
[13] J. Qin, X. Bian, S. Sl, W. Wang, Journal of Physics: Condensed Matter 10 (6) (1998) 1211.
[14] S. Das, J. Horbach, M. Koza, S. Mavila Chatoth, A. Meyer, Appl. Phys. Lett. 86 (1) (2005) 011918.
[15] O. Roik, O. Samsonnikov, V. Kazimirov, V. Sokolskii, S. Galushko, J. Mol. Liq. 151 (1) (2010) 42–49.
[16] P. Wang, Y.Q. Bu, J.B. Liu, Q.Q. Li, H.T. Wang, W. Yang, Mater Today 37 (2020) 64–73.
[17] A. Norman, P. Prangnell, R. McEwen, Acta Mater 46 (16) (1998) 5715–5732.
[18] K. Hyde, A. Norman, P. Prangnell, Acta Mater 49 (8) (2001) 1327–1337.
[19] S. Costa, H. Puga, J. Barbosa, A. Pinto, Mater. Des. 42 (2012) 347–352.
[20] V. Zakharov, Met. Sci. Heat Treat. 45 (7) (2003) 246–253.
[21] Y.L. Zhao, W.W. Zhang, B. Koe, W. Du, M.M. Wang, W.L. Wang, E. Boller, A. Rack, Z.Z. Sun, D. Shu, B.D. Sun, J.W. Mi, Mater. Charact. 164 (2020) 110353.
[22] Y.J. Huang, J.C. Khong, T. Connolley, J. Mi, Appl. Phys. Lett. 104 (3) (2014) 031912.
[23] A.P. Hammersley, J. Appl. Crystallogr. 49 (2) (2016) 646–652.
[24] A. Soper, N. Gudrun, X. Gudrun, Rutherford Appleton Laboratory Technical report: RAL-TR-2011-013. https://epubs. stfc. ac. uk/work/56240 (2011).
[25] A. Soper, Phys. Rev. B 72 (10) (2005) 104204.
[26] J. Røyset, N. Ryum, Int. Mater. Rev. 50 (1) (2005) 19–44.
[27] W.D. Callister, D.G. Rethwisch, Fundamentals of Materials Science and Engineering: An Integrated Approach, fifth ed., ISBN: 978-1-119-17550-6, John Wiley & Sons, Inc., Hoboken, 2018, pp. 333-337.
[28] A.K. Soper, Chem. Phys. 202 (2–3) (1996) 295–306.
[29] F.t. Frank, J. Kasper, Acta Crystallogr. 12 (7) (1959) 483–499.
[30] J. Ding, Y.Q. Cheng, E. Ma, Acta Mater 69 (2014) 343–354.
[31] M. Lee, C.M. Lee, K.R. Lee, E. Ma, J.C. Lee, Acta Mater 59 (1) (2011) 159–170.
[32] H. Lou, X. Wang, Q. Cao, D. Zhang, J. Zhang, T. Hu, H.K. Mao, J.Z. Jiang, Proc. Natl. Acad. Sci. U. S. A. 110 (25) (2013) 10068–10072.
[33] T. Kawasaki, H. Tanaka, Proc. Natl. Acad. Sci. U. S. A 107 (32) (2010) 14036–14041.
[34] A. Hirata, L. Kang, T. Fujita, B. Klumov, K. Matsue, M. Kotani, A. Yavari, M. Chen, Science 341 (6144) (2013) 376–379.
[35] A.C. Redfield, A. Zangwill, Phys. Rev. Lett. 58 (22) (1987) 2322.
[36] C. Desgranges, J. Delhommelle, Phys. Rev. Lett. 123 (19) (2019) 195701.